

# **Influence Of Hydroxyapatite On Zinc Tungstate (Hap/Znwo<sub>4</sub>) Nanoparticles And Its Antimicrobial Properties**

Nithya R<sup>1</sup>, Ayyappan S<sup>2</sup>

Department of Physics, Government College of Engineering, Salem, India

---

## **Abstract**

*In this study, we report the synthesis of nanocomposite material composed of zinc tungstate (ZnWO<sub>4</sub>) and Hydroxyapatite (HAp/ZnWO<sub>4</sub>) nanocomposite by a simple hydrothermal method. The prepared nanocomposites have been characterized by XRD, FESEM, HRTEM, EDX analysis, photoluminescence spectroscopy (PL) and UV-Visible spectroscopy. Prominent band edge emission of HAp-ZnWO<sub>4</sub> nanorods observed from PL confirmed the significant reduction in photogenerated charge carriers with doping of donor impurities. The higher activity of HAp/ZnWO<sub>4</sub> nanorods compared HAp may be due to their enlarged surface area which enhances the photogeneration of active OH<sup>-</sup> radicals in water. The as-synthesized g-C<sub>3</sub>N<sub>4</sub>/ZnWO<sub>4</sub> nanocomposite were analyzed its antibacterial properties against Gram-positive and Gram-negative clinical pathogens like E.coli and S.aures bacterial strain.*

---

Date of Submission: 11-11-2023

Date of Acceptance: 20-11-2023

---

## **I. Introduction**

The exploration for suitable semiconductor photo catalysts for effective utilization of solar energy to chemical energy is one of the noble missions of the scientific community. Hydroxyapatites (HAPs) ceramics are currently regarded as a highly significant class of materials in the fields of science, biology, and medicine. They are extensively utilized in chromatography and as nanostructured heterogeneous catalysts for oxidation reactions. Furthermore, extensive research has demonstrated the efficacy of these materials in environmental applications, specifically in the removal of diverse species from contaminated water and soil [1,2]. Additionally, they have proven to be efficient photocatalysts for the degradation of organic pollutants. HAP-based ceramics exhibit enhanced fixation to the surrounding tissue upon implantation in the human body due to the development of a fibrous layer devoid of tissue on their surface. The powdered form of hydroxyapatite (HAP) with nanometric particle size exhibits enhanced physicochemical and mechanical properties, including increased density, specific surface area, bioactivity, and sinterability. The physical properties of HAPs can be influenced by the presence of impurities, which can either be beneficial or detrimental. Certain cations found in bones play an active role in both the formation and reabsorption of bone tissue. The deficiency of W ions has been observed to decrease the growth rate of osteoblasts, resulting in a decrease in bone mass density. The rise of antibiotic-resistant bacterial strains poses a significant health problem, given that germs constitute a prominent contributor to chronic illnesses and mortality rates globally. Hence, it is crucial to prioritize the advancement of innovative and effective antibacterial agents [1]. Antimicrobial drugs targeting both gram-positive and gram-negative bacteria have been developed using a variety of inorganic and organic chemicals, as well as their combinations. A wide range of antimicrobial inorganic materials have been studied, including oxides like titanium oxide, silver oxide, and zinc oxide, as well as phosphates like pure hydroxyapatite (HAp) and HAp doped with various cations such as zinc, silver, cerium, strontium, copper, and titanium. These materials have been the subject of extensive research. Hydroxyapatite (HAp), a calcium phosphate compound with the chemical formula Ca<sub>10</sub>(PO<sub>4</sub>)<sub>6</sub>(OH)<sub>2</sub>, is an inorganic biomaterial that exhibits significant promise for many biomedical applications, particularly in the field of dentistry. This is mostly due to its exceptional biocompatibility, bioactivity, and osteoconductivity, as supported by previous research [18]. Various chemical modification techniques, such as cationic and anionic doping, can enhance the biological and physicochemical features of synthetic hydroxyapatite (HAp) [19, 20]. The introduction of dopants into the HAp network has the potential to influence various properties of the material, including its crystallinity, particle shape, surface charges, dissolution rates, densification, mechanical resistance, and thermal stability.

## II. Materials and Reagents

Calcium chloride di-hydrate ( $\text{CaCl}_2 \cdot 2\text{H}_2\text{O}$ ), di-ammonium hydrogen phosphate ( $(\text{NH}_4)_2(\text{HPO}_4)$ ) were purchased from Sigma Aldrich. Potassium permanganate ( $\text{KMnO}_4$ ), sodium nitrate ( $\text{NaNO}_3$ ), sulphuric acid ( $\text{H}_2\text{SO}_4$  98%), hydrogen peroxide ( $\text{H}_2\text{O}_2$ ), ammonium hydroxide ( $\text{NH}_4\text{OH}$ ) and ethanol were purchased from HI media Laboratory, India. All the chemicals were of analytical grade and used without further purification.

### Preparation of Pure HAp NPs

Hydroxyapatite (HAp) was synthesized by the chemical precipitation method. 3.7 g of calcium hydroxide was dissolved with 50 ml of distilled water, and 2.9 g of orthophosphoric acid was dissolved with 50 ml of distilled water. Both solutions were stirred for 30 minutes. Then the orthophosphoric acid was added drop-wise into the calcium hydroxide solution and stirred for 30 minutes; this was followed by adding NaOH solution drop-wise to maintain the pH level at 12. This was continuously stirred for half an hour. The mixture was allowed to settle; then, the precipitate was washed with double distilled water and finally it was kept in a microwave oven at 75 W for 20 minutes. Then it was kept in a muffle furnace for 4 hours. The dried sample was ground in a mortar to get white color pure Hydroxyapatite nanoparticles.

### Preparation of HAp/ZnWO<sub>4</sub> composites

The typical preparation of HAp/ZnWO<sub>4</sub> photocatalysts was as follows: an appropriate amount of HAp was completely dispersed in methanol assisted by ultrasonication. The as-prepared ZnWO<sub>4</sub> powder was subsequently added into the above solution and stirred for 24 h. The obtained sample was collected and washed with ethanol and distilled water; finally the samples were obtained by dried at 100°C for 4 h. According to this method, different mass ratios of HAp/ZnWO<sub>4</sub> from 3% to 7% were synthesized.

## III. RESULT AND DISCUSSION

### XRD Analysis

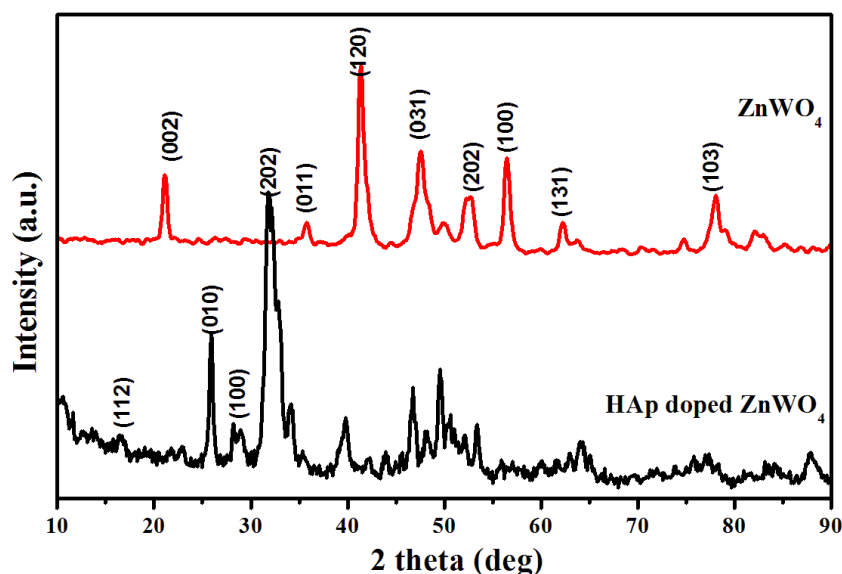
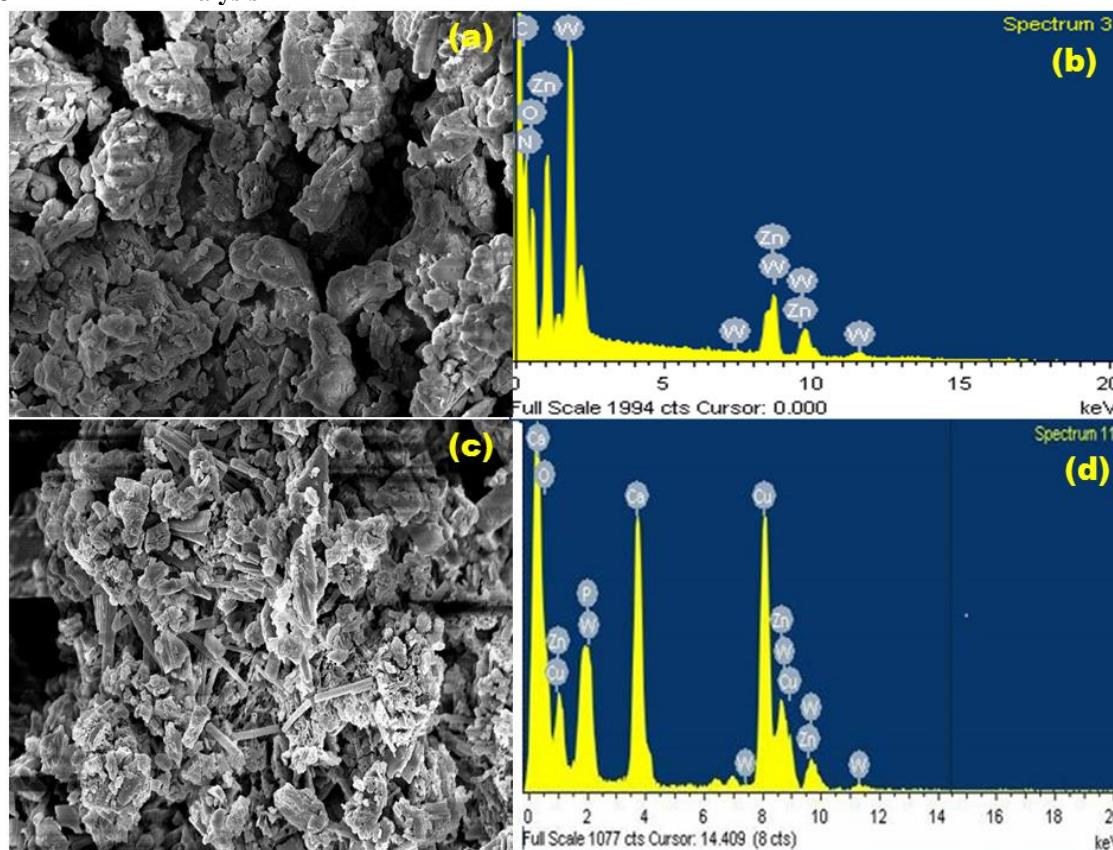


Figure. 1 XRD pattern of ZnWO<sub>4</sub> and HAp/ZnWO<sub>4</sub> nanorods

X-ray diffraction spectroscopy was employed to examine the crystal structures of the nanoparticles in their as-prepared state. Figure 1. This presentation illustrates the characteristic X-ray diffraction (XRD) pattern of porous nanorods composed of ZnWO<sub>4</sub> with included hydroxyapatite (HAp). Based on X-ray diffraction (XRD) analysis, it can be inferred that the prominent peak observed at an angle of  $2\theta=37.3^\circ$  corresponds to the characteristic diffraction of bulk hydroxyapatite (HAp) along the (002) crystallographic plane. However, for the exfoliated one-dimensional (1D) HAp nanorods, the peak is observed at a higher angle of  $2\theta=31.8^\circ$ , indicating a shift towards a greater diffraction angle. An evident reduction in the overall intensity was found, suggesting a corresponding drop in the interplanar stacking of the one-dimensional hydroxyapatite (HAp) nanostructures. The peak at around  $11.2^\circ$  is associated with the (100) plane of tri-s-triazine units, as reported by Meng et al. in 2018. The diffraction planes of pristine hydroxyapatite (HAp) have a strong resemblance to the graphitic carbon nitride (JCPDS 09-0432) in terms of their structural characteristics. The diffractogram acquired clearly exhibits the presence of many facets and orientations in the final result. According to Feng et al. (2016), the use of

chemical exfoliation on bulk hydroxyapatite (HAp) results in a reduction of the Van der Waals interaction between atoms, as well as an enhancement in the crystallinity of zinc tungstate ( $ZnWO_4$ ) by minimizing the exposed cross-plane diffusion of atoms. The observed diffraction peaks at angles of  $11.1^\circ$ ,  $23.7^\circ$ ,  $31.5^\circ$ ,  $36.2^\circ$ ,  $45.7^\circ$ ,  $57.5^\circ$ , and  $62.7^\circ$  can be attributed to specific crystallographic planes, namely (0 0 2), (1 0 0), (0 0 2), (0 1 1), (1 0 2), (1 1 0), (1 0 3), and (1 1 1), respectively. These peaks correspond to the crystal structure of  $ZnWO_4$  and are consistent with the hkl values specified in the standard card (JCPDS 15-0774). No additional secondary peaks were observed. The presence of distinct and prominent reflection peaks indicates that the HAp linked  $ZnWO_4$  nanorods exhibit a high degree of crystallinity. The compact arrangement can be attributed to the confinement of electrons and enhanced interlayer bonding. The Debye-Scherer method was employed to determine the crystallite size of both undoped and doped nanoparticles, yielding a range of 80 nm.

#### FESEM – EDAX Analysis



**Figure. 2 FESEM and EDAX Micrograph of HAp/ZnWO<sub>4</sub> nanoparticles**

The morphology of zinc tungstate ( $ZnWO_4$ ) nanorods doped with hydroxyapatite (HAp) was examined using field emission scanning electron microscopy (FESEM). As seen in Figure 2. In the sample, there is a significant presence of packing layers including nanorods and nanoparticles of varying sizes, which prominently display plate-like and irregular shapes. The field emission scanning electron microscopy (FESEM) micrograph reveals that the HAp/ $ZnWO_4$  composite, synthesized using thiourea, exhibits a morphology characterized by uniform and planar layers composed of densely packed and thick nanorods with an uneven configuration. The field emission scanning electron microscopy (FESEM) image of the  $ZnWO_4$  nanorods combined with highly calcium -enriched HAp indicates that the resulting product exhibits quasi-thin hexagonal rod morphology. The EDAX analysis has provided confirmation of the existence of Calcium (Ca), Phosphate (P), Carbon (C), and Nitrogen (N) in the HAp/ $ZnWO_4$  nanoparticulate. Additionally, a minimal amount of oxygen (O) was detected, along with the presence of Zinc (Zn) and Tungsten (W). The EDAX spectrum clearly indicates that the produced sample is devoid of contaminants. The presence of oxygen content can be attributed to the excessive moisture content present in the sample. The nanocomposite that was created contained components that were nearly stoichiometric in composition.

## HRTEM Analysis

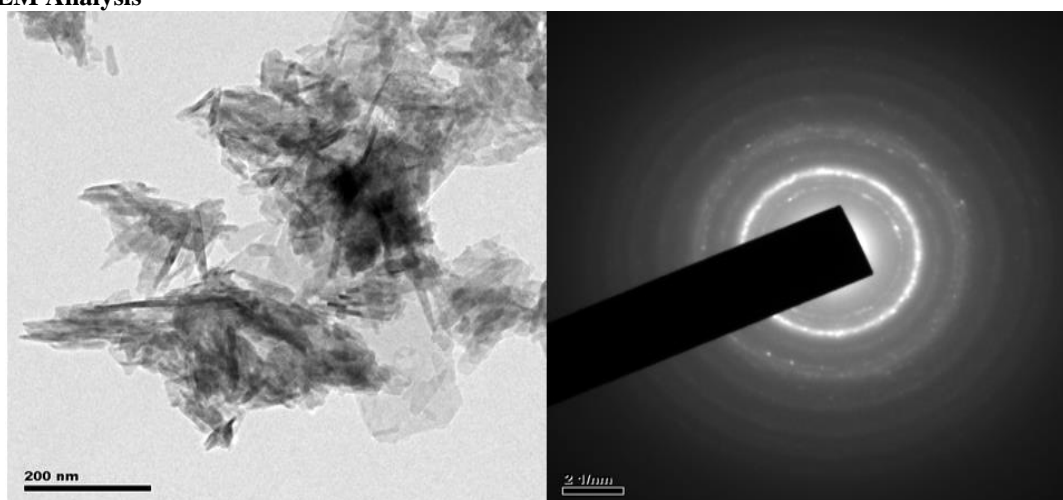


Figure. 3 HRTEM image of HAp/ZnWO<sub>4</sub> nanorods

Fig (3) shows the HRTEM micrographs and selected area electron diffraction pattern (SAED) of HAp doped ZnWO<sub>4</sub> nanorods. It is seen from the image, particles are found to be hexagon in shape with uneven size distribution ranging from 50 - 100 nm. The particle size calculated in this study is well-matched with the particle size calculated from XRD. The formation of particle agglomeration due to the reaction rate, hydroxyl impurities, charges of the particles and the solubility product constants. There is no major variation observed in the size and shape of the samples is observed due to the incorporation of dopant on the ZnWO<sub>4</sub> host structure. The g-C<sub>3</sub>N<sub>4</sub> coupled ZnWO<sub>4</sub> porous rod-like heterostructure obtained was well distributed on the surface. The SAED pattern confirms the improved crystalline nature of the as-prepared HAp coupled ZnWO<sub>4</sub> nanocomposite which is due to the addition of a dopant and large specific surface area of transition metal-doped nanoparticles.

## UV-Visible spectroscopy

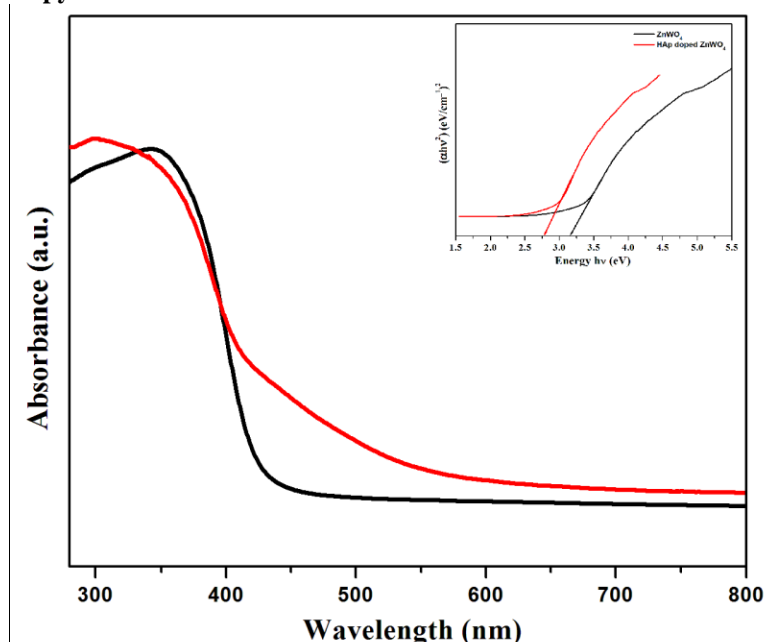


Figure 3 UV-Visible spectra of ZnWO<sub>4</sub> and HAp/ZnWO<sub>4</sub> nanorods

UV-Visible Diffused Reflection Spectroscopy was used to investigate the optical characteristics of nanoparticles. Fig. 4 shows the absorption spectrum of as-prepared and HAp coupled ZnWO<sub>4</sub> nanorods, which exhibit excellent visible light absorption and the absorption edges of the samples, shift apparently to a shorter wavelength. As prepared pristine HAp has a band edge at 450 nm and HAp coupled ZnWO<sub>4</sub> nanorods has the band edge at 400 nm. By doping HAp on to the ZnWO<sub>4</sub> transition metal oxide host structure, the absorption

edge of HAp coupled ZnWO<sub>4</sub> nanocomposite has a clear monotonic blue shift and probable reason may be due to a perfect lattice stacking of HAp on ZnWO<sub>4</sub> crystallite and quantum confinement effect that modifies the position of conduction and valence band edges. The UV-absorption spectrum of HAp doped ZnWO<sub>4</sub> nanocomposite shifted towards lower wavelength was due to the passivation of functional groups. The bandgap energy ( $E_g$ ) which can be estimated by plotting the tauc plot of  $(\alpha h\nu)^{1/2}$  versus photo energy ( $E_g$ ). This indicates that the prepared HAp coupled ZnWO<sub>4</sub> nanocomposite could absorb both UV and visible range spectra, which may be due to an internal lattice defects. With the effect of HAp coupling on to the ZnWO<sub>4</sub> photocatalytic activity of the nanocomposite was enhanced due to wide visible light harvesting. Thereby, the intensity of the UV-absorption spectrum of HAp/ ZnWO<sub>4</sub> increases and the creation of electron-hole pairs on the heterogeneous interface may also significantly increased due to visible light irradiation.

### PL Spectroscopy

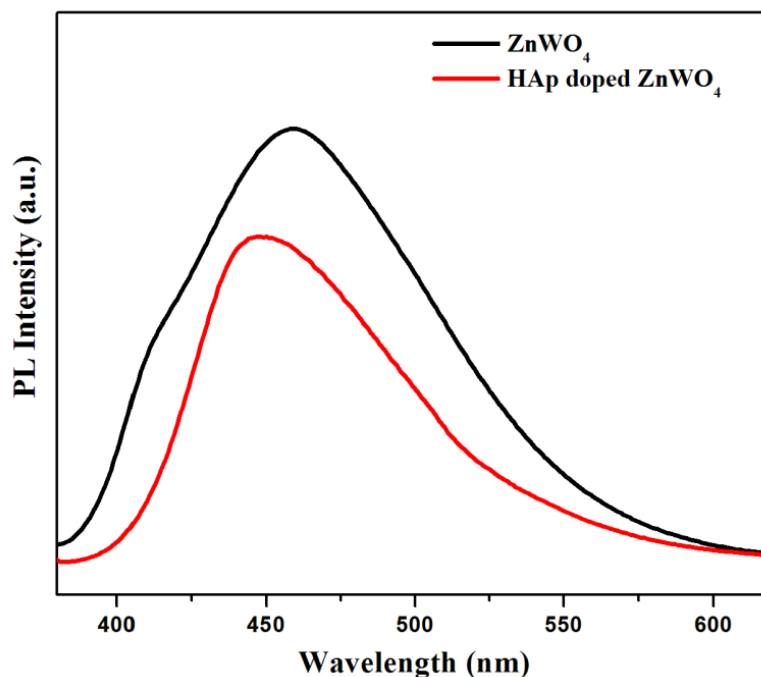


Figure 5 PL spectra of ZnWO<sub>4</sub> and HAp/ZnWO<sub>4</sub> nanorods

The broad PL band from ZnWO<sub>4</sub> host is often attributed to the charge transfer between oxygen and tungsten ions in [WO<sub>6</sub>]<sub>6</sub> molecular complex. The origins of PL can be classified into band edge emission and defect emission. Due to the large difference between the bandgap of ZnWO<sub>4</sub> (about 3.21 eV) and its emission energy (around 2.83eV), we can exclude the possibility of band edge recombination as the candidate of the broadband emissions of ZnWO<sub>4</sub> grains. It is observed that ZnWO<sub>4</sub> nanograins, where coordinately unsaturated vacancies are active sites for luminescence. This feature allows us to assign the broad PL band peaking at about 480 nm to certain kinds of defects in ZnWO<sub>4</sub>. The most common defects in ZnWO<sub>4</sub> include O, W, and Zn vacancies, which are likely candidates of the luminescence centers. Although the relation between the intrinsic defects and the luminescence centers in ZnWO<sub>4</sub> are not clearly identified yet, the PL spectra in Figure demonstrate that the PL properties of ZnWO<sub>4</sub> host are highly governed by the number and the kind of defects in ZnWO<sub>4</sub> lattice.

### Antibacterial Activity

Figure. 6 shows the antibacterial characteristics of both as-synthesized pristine hydroxyapatite (HAp) and HAp/ZnWO<sub>4</sub> nanocomposite were examined in this study. The antibacterial activity of these materials was tested against Gram-positive bacteria. Our findings demonstrate that the incorporation of ZnWO<sub>4</sub> into HAp resulted in enhanced inhibitory effects, as seen by larger zone diameters compared to pristine HAp. The HAp/ZnWO<sub>4</sub> nanocomposite exhibited a significant Zone of Inhibition (ZOI) against E.coli at an ideal concentration of 100µg/disk. This high inhibitory effect can be attributed to the physicochemical interaction between the HAp/ZnWO<sub>4</sub> nanocomposite and the bacterial surface. The presence of a refined crystalline structure facilitates the efficient transport of photogenerated electron-hole pairs from the core shells to the catalytic surface. This, in turn, boosts the antibacterial properties of the nanocomposite material that is created.

The absorption of visible wavelengths by pure HAp and HAp/ZnWO<sub>4</sub> nanoparticles results in the generation of photogenerated electron-hole pairs. The photogenerated free radicals interact with alkaline chemicals found on the surface, resulting in their conversion into hydroxyl ions (OH<sup>-</sup>) and superoxide radicals (O<sub>2</sub><sup>\*</sup>). This chemical transformation has an impact on the bacterial cell membrane. Furthermore, it has been noted that hydroxyapatite (HAp) exhibits the ability to permeate bacterial cells, thereby impeding their proliferation.

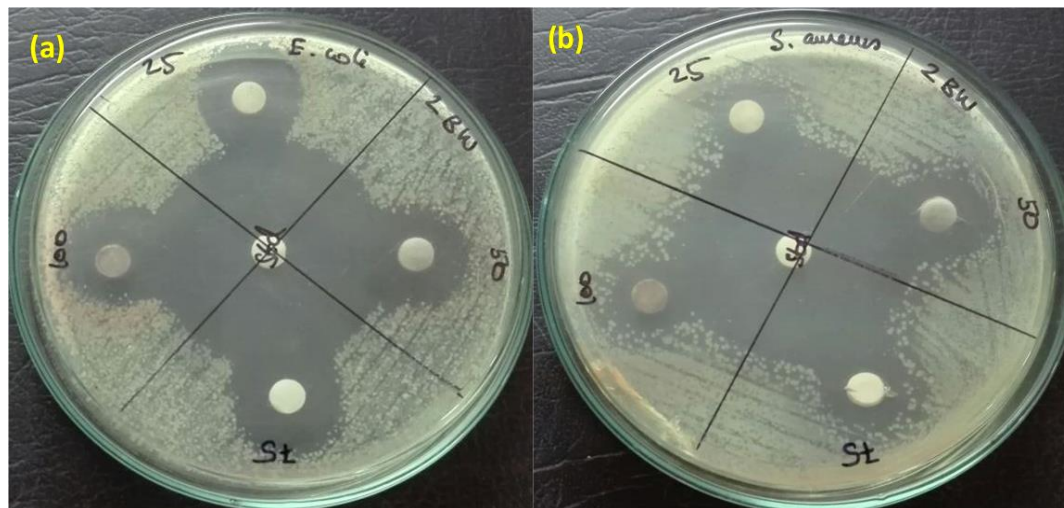


**Figure 6 ZOI of HAp/ZnWO<sub>4</sub> nanoparticles against E.coli and S.aures**

#### IV. Conclusion

In conclusion, hydrothermal method is very ease and cost effective to synthesize the HAp doped ZnWO<sub>4</sub>. The analysis of XRD, HRTEM showed that particles of all samples are of nano size and homogenous in structure. From the XRD data the crystallite size is observed to decrease with the increase content of Zn. This is due to the decrease in volume density of the atom. The intensity of the band decreases by the addition of Cu dopant to the HAp. The Ca-deficiency occurs because of the W-doping process, and increases with addition of the dopants. The antibacterial activity of the HAp/ZnWO<sub>4</sub> nanoparticles depended strongly on their Zn<sup>2+</sup> content. Thus, the use of a bio template and Zn<sup>2+</sup> ions is an efficient approach for the formation of novel HAp-based biomaterials with promising antibacterial properties. This synthesis approach will pave a new pathway for the functionalization of other materials for different biomedical applications.

#### REFERENCE

- [1]. Ding, W, Wu, X & Lu, Q 2019, 'Structure And Photocatalytic Activity Of Thin-Walled Cuwo<sub>4</sub> Nanotubes: An Experimental And DFT Study', Mater. Lett, Vol. 253, Pp. 323-326.
- [2]. Dong, P, Hou, G, Xi, X, Shao, R & Dong, F 2017, 'WO<sub>3</sub>-Based Photocatalysts: Morphology Control, Activity Enhancement And Multifunctional Applications', Environ. Sci. Nano. Vol. 4, Pp. 539-557.
- [3]. El-Khatib, M, Doma, AS, Abo-Zaid, GA, Badawi, MS, Mohamed, MM & Mohamed, AS 2020, 'Antibacterial Activity Of Some Nanoparticles Prepared By Double Arc Discharge Method', Nano-Structures & Nano-Objects, Vol. 23, P. 100473.
- [4]. Huang, K, Hong, Y, Yan, X, Huang, C, Chen, J, Chena, M, Shia, W & Liu, C 2016, 'Hydrothermal Synthesis Of Hap/Cdwo<sub>4</sub> Nanocomposite And Enhanced Photocatalytic Activity For Tetracycline Degradation Under Visible Light', Cryst. Eng. Comm. Vol. 18, Pp.6453-6463.
- [5]. Kolahalam, LA, Viswanath, IK, Diwakar, BS, Govindh, B, Reddy, VY & Murthy, LN 2019, 'Review On Nanomaterials: Synthesis And Applications', Mater. Today: Proc. Vol. 18, Pp. 2182-2190.
- [6]. Lester, E, Dunne, P, Chen, Y & Al-Atta, A 2018, 'The Engineering Of Continuous Hydrothermal/Solvothermal Synthesis Of Nanomaterials', Supercritical And Other High-Pressure Solvent Systems, Pp.416-448.
- [7]. Li, M, Xu, Y, Tu, WG, Chen, G & Xu, R 2017, 'Metal-Free Photocatalysts For Various Applications In Energy Conversion And Environmental Purification, Green', Chem. Vol. 19, Pp. 882-899.
- [8]. Liu, K, Li, J, Yan, X & Shi, W 2017, 'Synthesis Of Direct Z-Scheme Mnwo4/G-C3N4 Photocatalyst With Enhanced Visible-Light Photocatalytic Activity', Nano, Vol. 12(10), P. 1750129.
- [9]. Parashar, M, Shukla, VK & Singh, R 2020, 'Metal Oxides Nanoparticles Via Sol-Gel Method: A Review On Synthesis, Characterization And Applications', Jour.Of. Mater. Sci: Mater In Electr, Vol. 31(5), Pp. 3729-3749.
- [10]. Parthibavarman, M, Karthik, M, Sathishkumar, P & Poonguzhali, R 2018, 'Rapid Synthesis Of Novel Cr-Doped WO3 Nanorods: An Efficient Electrochemical And Photocatalytic Performance', Journal Of The Iranian Chemical Society. Vol. 15, Pp. 1419-1430.
- [11]. Pereira, PFS, Gouveia, AF, Assis, M, Oliveira, RCD, Pinatti, IM, Penha, M, Goncalves, RF, Gracia, L, Andresd, J & Longoa, E 2018, 'Znwo4 Nanocrystals: Synthesis, Morphology, Photoluminescence And Photocatalytic Properties', Phys. Chem. Chem. Phys. Vol. 20, Pp. 1923-1937.
- [12]. Pilli, SK, Deutsch, TG, Furtak, TE, Brown, LD, Turner, JA & Herring,AM 2013, 'Bivo4/Cuwo4 Heterojunction Photoanodes For Efficient Solar Driven Water Oxidation', Physical Chemistry Chemical Physics, Vol. 15, Pp. 3273-3278.
- [13]. Yang, G & Park, SJ 2019, 'Conventional And Microwave Hydrothermal Synthesis And Application Of Functional Materials', A Review. Materials, Vol. 12(7), P. 1177.

- [14]. Ben-Arfa, B. A. E., Salvado, I. M. M., Ferreira, J. M. F., And Pullar, R. C., 2017, Novel Route For Rapid Sol-Gel Synthesis Of Hydroxyapatite, Avoiding Ageing And Using Fast Drying With A 50-Fold To 200-Fold Reduction In Process Time: *Materials Science And Engineering C*, V. 70, P. 796–804.
- [15]. Bharath, G., Madhu, R., Chen, S. M., Veeramani, V., Mangalaraj, D., And Ponpandian, N., 2015, Solvent-Free Mechanochemical Synthesis Of Graphene Oxide And Fe<sup>3+</sup>/O<sup>4-</sup>-Reduced Graphene Oxide Nanocomposites For Sensitive Detection Of Nitrite: 15529–15539 P.
- [16]. Capanema, N. S. V., Mansur, A. A. P., Carvalho, S. M., Silva, A. R. P., Ciminelli, V. S., And Mansur, H. S., 2015, Niobium-Doped Hydroxyapatite Bioceramics: Synthesis, Characterization And In Vitro Cytocompatibility: *Materials*, V. 8, P. 4191–4209.
- [17]. Deepa, C., Begum, A N., And Aravindan, S., 2013, Preparation And Antimicrobial Observations Of Zinc Doped Nanohydroxyapatite: *Nanosystems: Physics, Chemistry, Mathematics*, V. 4, P. 370–377.
- [18]. Dong, X., And Cheng, F., 2015, Recent Development In Exfoliated Two-Dimensional G-C3n4nanosheets For Photocatalytic Applications: *Journal Of Materials Chemistry A*, V. 3, P. 23642–23652.
- [19]. Redoi, D., Iconaru, S. L., Deniaud, A., Chevallet, M., Michaud-Soret, I., Buton, N., And Prodan, A. M., 2017, Textural, Structural And Biological Evaluation Of Hydroxyapatite Doped With Zinc At Low Concentrations: *Materials*, V. 10.
- [20]. Ramadas, M., Bharath, G., Ponpandian, N., And Ballamurugan, A. M., 2017, Investigation On Biophysical Properties Of Hydroxyapatite/Graphene Oxide (Hap/GO) Based Binary Nanocomposite For Biomedical Applications: *Materials Chemistry And Physics*, V. 199, P. 179–184.
- [21]. Singh, V., Devi, S., Pandey, V. S., Bharj, R. S., And Tyagi, S., 2018, Synthesis And Characterization Of Carbon Nanotubes Doped Hydroxyapatite Nanoceramic For Orthopedic Applications: *Transactions Of The Indian Institute Of Metals*, V. 71, P. 177–183.